Nuclear Materials and Energy 34 (2023) 101368

Contents lists available at ScienceDirect

Nuclear Materials and Energy

journal homepage: www.elsevier.com/locate/nme

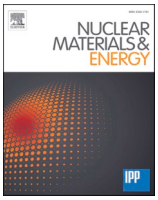

Investigation of the silicon coated film characteristics on tungsten surface in EAST fusion device

Yanhong Guan [a,b], Guizhong Zuo [a,*], Xiancai Meng [a,c,*], Wei Xu [c], Yaowei Yu [a], Ming Huang [a], Lin Li [a,b], Jiansheng Hu [a,d]

[a] Institute of Plasma Physics, Hefei Institutes of Physical Science, Chinese Academy of Sciences, Hefei, Anhui 230031, China
[b] University of Science and Technology of China, Hefei, Anhui 230026, China
[c] Institute of Energy, Hefei Comprehensive National Science Center, Hefei, Anhui 230026, China
[d] CAS key Laboratory of Photovoltaic and Energy Conservation Materials, Hefei 230031, China

ARTICLE INFO

Keywords:
Siliconization
Tungsten
Plasma
EAST

ABSTRACT

Siliconization using 10 % SiD_4 + 90 % He assisted by ion cyclotron range of frequency discharge (ICRF) or glow discharge (GD) was performed in EAST with full tungsten (W) diverters. It was found that the coated Si film on W sample at a higher baking temperature (160 °C) was smoother than that at a lower baking temperature (60 °C). This was mainly because physically adsorbed gaseous impurities were released at a higher baker temperature. This process improved the adhesion between the film and the surface of W. An increase in the ICRF working power from 20 kW to 40 kW further increased the Si content and the film thickness by 1.5 times. The cleaning efficiency of ICRF on the surface of the W sample before siliconization was higher at 40 kW than that at 20 kW, which facilitated the removal of oxides and other compounds from the surface of W. The ratio of silicon/oxygen (Si/O) and the thickness improved considerably due to greater ionization and deposition of SiD_4. Additionally, siliconization via GD was more uniform and 1.5 nm thicker than that via ICRF, which was because of the greater working gas pressure, coating duration, and homogeneity in GD. These results might be used as a reference for evaluating the effect of siliconization on plasma performance and its application in fusion devices.

1. Introduction

Nuclear fusion is a viable alternative to carbon-dependent energy sources [1]. To make power plants with nuclear fusion economically sustainable, maintaining high-performance plasma under steady-state conditions for long pulse durations in the fusion device is necessary [2]. However, plasma–material interaction (PMI) is a key issue in the realization of practical fusion power since the beginning of fusion research [3]. Fuel recycling and the presence of impurities arising from PMI produce long pulse and high-performance plasmas. High recycling and concentration of impurities in the plasma can degrade plasma confinement, causing uncontrollable changes in plasma density and disruptions. Thus, selecting a suitable plasma-facing material (PFM) and wall conditioning method can effectively decrease the PMI and improve performance of plasma.

Tungsten is a plasma-facing material and used in several fusion devices. In the future, it might also be used in ITER devices due to its high thermal conductivity, high melting point (3,680 K), and low sputtering rate [4–6]. After being commissioned in 2005, the EAST device was operated with graphite diverters for eight years up to 2012. When the heating power goes above 10 MW, the heat flux loaded on the diverters can increase rapidly over 10 MW m^{-2} for long pulse operations. To accommodate the high heat load in the EAST, the ITER-like W diverter was developed to be used as the upper and lower diverters in the EAST [7]. However, these diverters have several limitations, including W melting, cracking, and W impurity due to the strong interaction between W wall, and high-temperature plasma. The problems might erode and damage the wall material, causing plasma confinement degradation. Therefore, it needs to develop some wall conditionings to improve the W wall condition and mitigate the interaction between the W wall and high temperature plasma [8].

Some advanced wall conditioning technologies have been developed and widely used in fusion devices for processes such as baking, discharge cleaning, boronization, siliconization, and lithium coating [9]. Baking

* Corresponding authors at: Institute of Plasma Physics, Hefei Institutes of Physical Science, Chinese Academy of Sciences, Hefei, Anhui 230031, China (X.C. Meng).
E-mail addresses: zuoguizh@ipp.ac.cn (G. Zuo), xcmeng@ie.ah.cn (X. Meng).

https://doi.org/10.1016/j.nme.2023.101368
Received 10 October 2022; Received in revised form 8 January 2023; Accepted 15 January 2023
Available online 16 January 2023

can effectively desorb low-energy impurities (gaseous impurities adsorbed to the first wall, such as H_2O, CO_2, N_2, and O_2) from the wall materials. However, it is restricted by the baking temperature and duration and cannot eliminate high-energy impurities (binding energy > 2.5 eV) [10]. Discharge cleaning, including GDC and ICRF, might be used for decreasing impurities and stabilizing plasma. To further control impurities and fuel recycling and improve plasma performance, some wall coating methods, such as boronization [11], lithium (Li) coating [12], and siliconization [9], were used. These coatings were assisted by glow discharge (GD) and ion cyclotron range of frequency discharge (ICRF). Diborane(B_2H_6) [9], trimethylboron B $(CH_3)_3$ [13], decaborane $B_{10}H_{14}$ [14] and carboranes $C_2B_{10}H_{12}$ [15] have been applied for boronization in DIIID [11], LHD [16], and ASDEX [17], ASDEX Upgrade (AUG) [18], and EAST [9]; their application improved plasma performance. However, due to H has been introduced from these boranes, the H/(H + D) ratio kept very high, which has been observed in EAST [19]. Lithium coatings were applied using lithium evaporation and lithium-particle real-time injection to TFTR [20], EAST [21], and NSTX [22]. Lithium coatings effectively removed H isotopes and other impurities, which reduced particle recycling and improved plasma confinement. However, due to the short lifetime (~300 s) of Li and because most of the tritium present was captured by the Li coating, its application in future fusion devices was limited [23]. In TEXTOR and HL-1M, siliconization can reduce particle recycling by using a mixture (0.9 He + 0.1 SiH_4) [24,25]. For further reducing the release of H, and the ratio of H/(H + D), a new silane SiD_4 was proposed for application in siliconization on the full tungsten diverter in EAST. In this study, the main emphases are the comparison of the Si film characteristics on the tungsten material sample with various coating conditions, including baking temperature, ICRF power, and discharge types in EAST.

2. Experimental setup

Siliconization was normally conducted using a mixed gas of 10 % SiD_4 + 90 % He and assisted by ICRF or GD in EAST. The ICRF discharge was performed using a set of antenna located at the B window, corresponding to two sets of 50 kW RF transmitters. During ICRF discharge, ICRF power, and working pressure were set at 20–40 kW, and ~ 10^{-2} Pa, respectively, in the presence of a toroidal magnetic field (B_T) of ~ 0.2 T. The gas pressure was kept constant adjusted by feedback control system during ICRF discharge, and it means that removed impurity gas and part working gas would be pumped with ICRF-off phase. Due to overheating issue at the antenna and interface, the duty time was set at 0.5 s on/5 s off, which is usually for wall cleaning, i.e. to pump the released species without ionization. The glow discharge was performed using four fixed anodes, located at the P-A, B-C, F-G, and J-K windows. During glow discharge, each anode had a power of 400 W (2 A, 200 V), and the working pressure was ~ 10^{-1} Pa, with Bt = 0 T.

The tungsten (W) samples were in the form of sheets (13 mm × 10 mm × 1 mm), and the sample surface was mechanically polished using diamond powder. Before the coating experiments, all samples were cleaned ultrasonically with high-purity alcohol (99.9 %). The W samples were placed on an experimental platform in the Materials and Plasma Evaluation System (MAPES) located at the H port and inserted into the vacuum vessel at R = 2.356 m (main limiter located at R = 2.35 m) during siliconization. The angle of the magnetic field direction (θ) relative to the sample surface was ~1.5°. The MAPES consisted of diagnostics, a vacuum chamber, and cooling and heating systems [26]. Before siliconization, the W samples were inserted into a vacuum vessel of EAST using MAPES. Then, He-ICRF/GDC and baking (at 60 °C and 160 °C) were performed for about 30 min to remove gaseous impurities (e.g., H_2O and CO_2) by adsorption to the surface of W to achieve good substrate conditions. The coating duration of siliconization assisted by He-ICRF and He-GD was about 110 min. The working gas pressure with 10 % SiD_4 + 90 % He during siliconization by ICRF and GD was 0.01 Pa and 0.1 Pa, respectively. During siliconization, the W samples were baked at ~60 °C and 160 °C by the baking module of the MAPES. The power of He-ICRF was 20 and 40 kW, and the GD power was 1.6 kW. The experimental parameters are listed in Table 1.

After the Si coating experiment, the platform was withdrawn to the vacuum chamber of the MAPES. Then, the W samples with the Si film were placed in an Ar atmosphere. Scanning electron microscopy (SEM) and X-ray photoelectron spectroscopy (XPS) were performed to characterize the microstructural properties, thickness, and composition of the Si film. The XPS analyzed the elements of C, O, Si, and W. The samples were exposed to air before conducting the XPS analysis about 5 min. Thermal desorption spectroscopy (TDS) was performed to analyze the gaseous impurities released from these samples.

3. Results and discussion

3.1. Characteristics of the Si-coated film assisted by ICRF

The SEM micrograph of the W samples showed some spots, scratches, and scars on the surface before the coating experiment, which probably occurred because of mechanical polishing, as shown in Fig. 1. The dark spots indicated the presence of oxides.

The microstructure and the results of the XPS analysis of the surface of the W samples after performing siliconization via ICRF experiments at 20 kW working power and ~60 and 160 °C baking temperatures are shown in Fig. 2. The scars on the original W surface were covered by the Si film on both surfaces of the sample. As shown in Fig. 2(a), when the W substrate was exposed to a lower baking temperature, many bubbles and folds were formed on the film. Additionally, the diameter of the folds was 75–80 nm, and the ratio of the area of bubbles and folds to the whole surface area of the film was almost 60 %. These findings indicated that the adhesion between the film and the W surface was poor under this condition, and it could break or fall off if the film was bombarded by plasma. However, the film on the W substrate at a higher baking temperature (about 160 °C) was flat and smooth, and no bubbles and folds were formed (Fig. 2(b)). Thus, the adhesion between the film and the W surface was better at the higher baking temperature.

The distribution of the components in the film was analyzed by XPS (Fig. 2c and 2d). As shown in Fig. 2(c), the analysis to determine the distribution of the elements of the film on the W sample at ~60 °C and from 0 to 1.2 nm showed that the main elements on the film surface were C, O, Si, and W respectively. The content of C and O was higher than that of the other two elements, which had an obvious relationship with low baking temperature. Because most of CO_2 and H_2O impurity gases would still retain on the W sample after low temperature baking, which will be described in the discussion part in detail. When the Si coating, the impurity gases would react with Si film to form some compounds including C and O. In addition, due to He plasma sputtering, C and O on sample surface will be removed and redeposited with Si. Therefore, with the low temperature baking case, the C and O elements on the Si film surface were relatively high. From 1.2 to 3.0 nm, the content of C, O and Si decreased, while the content of W continued to increase. As shown in Fig. 2(d), from 0 to 0.6 nm, the content of Si and W increased, but the content of C and O decreased slightly. The content of Si was higher than that of the other elements including C and O because high temperature baking could effectively desorb gaseous impurities before Si coating, such as H_2O and CO_2. From 0.6 to 3.0 nm, the content of O increased to a peak value, and then decreased. The Si and C content decreased, while

Table 1
Experimental parameters of siliconization on tungsten surface.

	Power/kW	Pressure/Pa	Temperature/°C
Siliconization assisted by ICRF	20	0.01	~60
	20	0.01	160
	40	0.01	~60
Siliconization assisted by GD	1.6	0.1	160

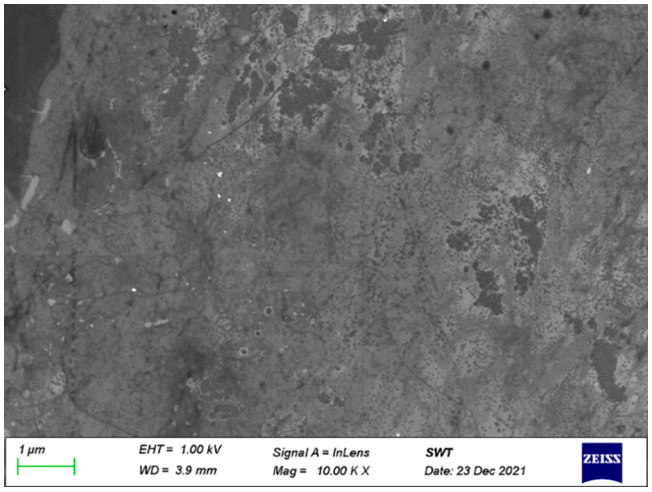

Fig. 1. The SEM image of the original W surface.

the content of W increased rapidly. After 3.0 nm, the decrease in the content of C and O weakened. When the content of Si was zero, the curve of W flattened, indicating that the Si film thickness on the W sample at 160 °C was also ~3.0 ± 0.1 nm.

We also analyzed the chemical properties of the coating with siliconization assisted by ICRF from six points at different depths, which were located at 0.0 nm, 1.2 nm, 2.4 nm, 3.6 nm, 4.8 nm, and 6.0 nm beneath the Si film surface, as shown in Fig. 3(a-c). As shown in the Si 2p spectra (Fig. 3(a)), at 60 °C, the Si 2p peaks appeared at 100.40 eV and 101.90 eV on the surface and 1.2 nm beneath the film surface, respectively, along with the binding energy peaks of O 1 s at 530.40 and 532.40 eV (as shown in Fig. 2(b)), which corresponded to SiO_2. This indicated that the oxidation reactions of Si could occur at low temperatures. However, the SiO_2 peak at 100.40 eV disappeared and the SiO_2 peaks at 99.50 eV and 101.90 eV were found on the surface of the film when the W sample was baked at 160 °C. Moreover, within 1.2 nm, only the peak of SiO_2 was detected at 101.90 eV. According to Fig. 2(c, d), the content of Si in the thickness range of 0–1.2 nm were the second and first constituents, corresponding to the backing temperature of W samples at 60 and 160 °C, respectively. This indicated that the content of Si increased when the W substrates were baked at a higher temperature during the coating test. Additionally, as shown in Fig. 3(c), the binding energy curves of the W 4f spectra were similar when the W samples were baked at 60 °C and 160 °C. The WO_2 and WO_3 peaks at 31.37 eV and 33.56 eV, respectively, along with the O 1 s peaks at 530.40 and 532.4 eV from 2.4 to 3.0 nm of the film were attributed to the oxidization of the surface before the experiment. In this experiment, the quality of Si coating was defined through morphology, thickness and component. The surface of film was smoother, the thickness was thicker and the content of Si improved, such film was defined high quality. Thus, based on the results of the SEM and XPS analysis, it can draw the conclusion that the W substrates at a higher temperature can improve the quality of the Si coating.

The SEM images and XPS characterization results of siliconization via ICRF at 60 °C and higher working power of 40 kW are shown in Fig. 4. As shown in Fig. 4(a), after siliconization, the surface of the W sample was uniformly covered by the Si film. Compared to the results described previously (Fig. 1), the scratches and scars on the W surface disappeared due to the formation of the coated Si film. Compared to the number of bubbles and folds described in Fig. 2 (a), almost no bubbles and folds were visible, which was similar to the findings described in Fig. 2(b), where the surface had a smooth and compact microstructure. These findings indicated that the higher working power of ICRF can enhance the adhesion of the film and the W surface.

As shown in Fig. 4(b), from 0 to 1.2 nm, the content of Si increased rapidly and reached a peak value, which was higher than that of C, O and W. The content of C and O decreased and W increased slightly.

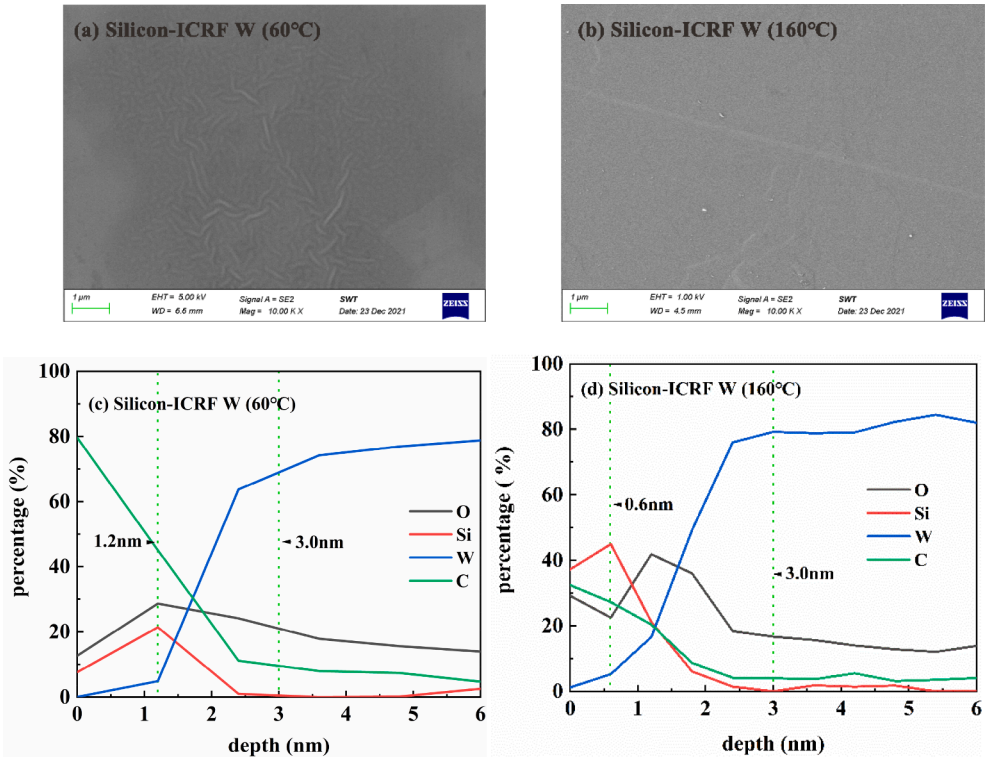

Fig. 2. The SEM images and the results of the XPS analysis of the surface of the W samples for Si coating via ICRF at 20 kW working power and 60 °C and 160 °C baking temperature: (a) the microstructure of the Si film at 60 °C; (b) the microstructure of the Si film at 160 °C; (c) the distribution of elements with film thickness at 60 °C; (d) the distribution of elements with film thickness at 160 °C.

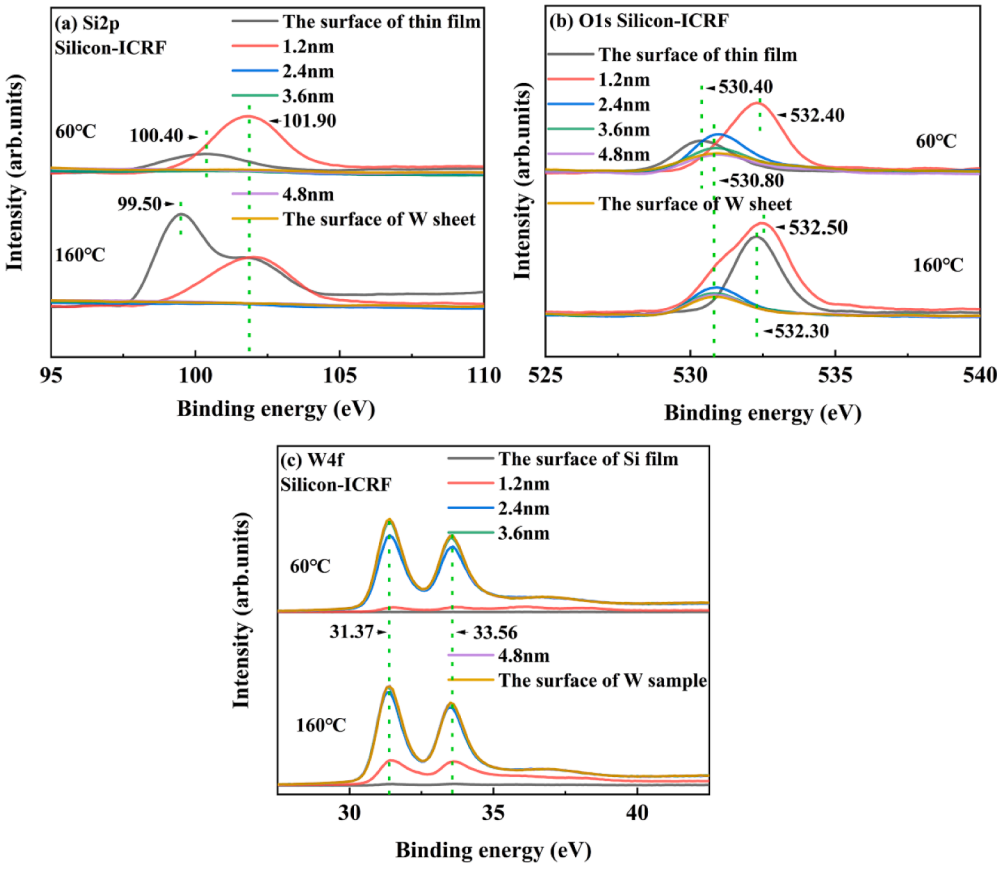

Fig. 3. The XPS spectra of the Si coating on the W samples via ICRF at 20 kW working power and 60 °C and 160 °C baking temperature: (a) Si 2p spectra; (b) O 1 s spectra; (c) W 4f spectra.

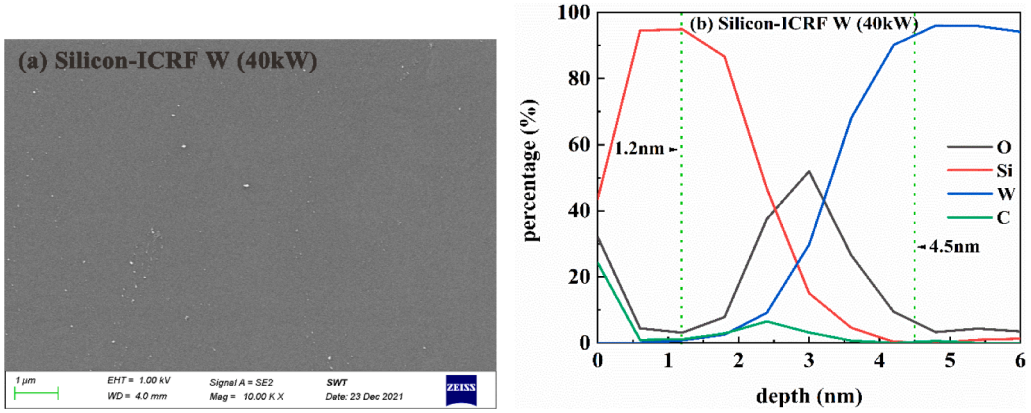

Fig. 4. The SEM images and the results of the XPS analysis of Si coating on the surface of the W samples performed by ICRF at 40 kW working power and 60 °C baking temperature: (a) the microstructure of the film; (b) the distribution of the elements with film thickness.

Additionally, from 1.2 to 4.5 nm, the content of Si decreased rapidly and almost became zero. The content of C and O increased and reached a peak value rapidly and then declined, while the content of W increased rapidly. After 4.5 nm, the curves of the contents of C, O, Si, and W became flat. These results showed that the thickness of the film that coated the W sample baked at 60 °C and 40 kW ICRF working power was ~4.5 ± 0.1 nm, which was thicker than the film that coated the sample at 20 kW working power of the ICRF.

The results of the analysis of the chemical properties of the Si-coated W samples after siliconization, assisted by ICRF are shown in Fig. 5(a-c). As described in the previous experiment, we selected six points beneath the surface of the film (1.2 nm, 2.4 nm, 3.6 nm, 4.8 nm, and 6.0 nm) to conduct the analysis. As shown in Fig. 5(a), the Si 2p spectra were located around 97–105 eV. For the surface of the Si film, there were two peaks located at 99.30 eV and 103.00 eV (along with the O 1 s spectral peak at 532.4 eV (Fig. 5(b))), respectively, which corresponded to SiO_2. These spectra indicated that the surface of the Si film was slightly oxidized while being transferred to the XPS system in the air. From 1.2 to 2.4 nm, only the Si peaks located at 99.30 eV and 102.00 eV were observed. The Si 2p spectra of the remaining three positions showed no significant peaks. These results suggested that the main component of the film was Si. Additionally, as shown in Fig. 5(c), the W 4f spectra were in the region of 29–39 eV. From the surface to a depth of 1.2 nm, the curves of the W 4f spectra were flat. From a depth of 2.4 nm to the

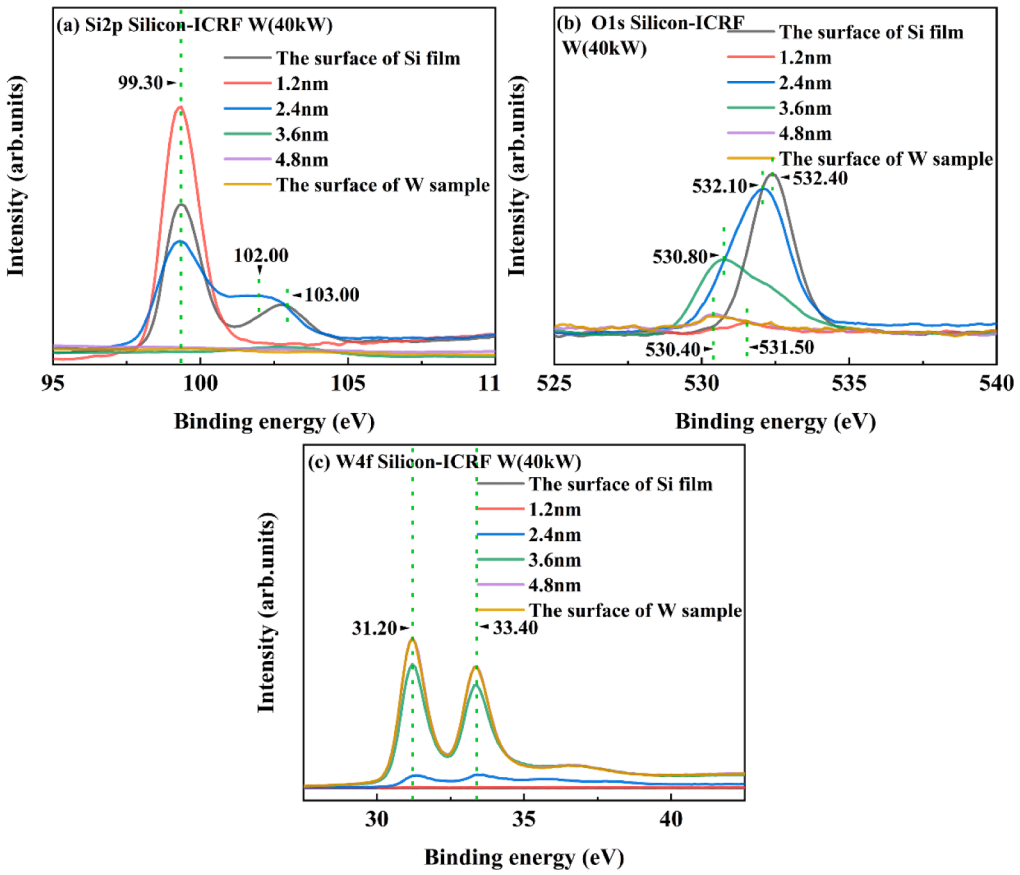

Fig. 5. The XPS spectra of the Si coating on the surface of the W sample formed by ICRF at 40 kW working power and 60 °C baking temperature: (a) Si 2p spectra; (b) O 1 s spectra; (c) W 4f spectra.

surface of the W sample, two peaks were detected at 31.20 eV and 33.40 eV. These peaks corresponded to W and WO_2, respectively, which were different from WO_2 and WO_3 on the surface of the W samples, as shown in Fig. 3(c). These findings indicated that the oxidized surface of the W sample was cleaner when ICRF was applied with higher working power. Based on these results, we concluded that high working power can increase the thickness of the film and the content of Si.

3.2. Characteristics of the Si-coated film assisted by GD

The SEM images and results of the XPS analysis of Si-coated samples produced by conducting GD at 160 °C baking temperature and 1.6 kW operating power are shown in Fig. 6. The morphology of the film deposited on the W sample was smooth and compact and the scratches were too small for analysis. Also, no grain or bubble was found on the surface of the Si coating, as shown in Fig. 6(a). The composition of the Si-coated samples was obtained by XPS. As shown in Fig. 6(b), from 0 to 1.8 nm, the content of O and C decreased. The content of Si rapidly increased and reached a peak value and the content of W changed slowly. After 1.8 nm, the content of C slowly increased and arrived stability, the content of Si decreased and approached zero at 6.0 nm, the content of W increased quickly, but the content of O maintained a balance. These results showed that the thickness of the coated film was ~ 6.0 ± 0.1 nm.

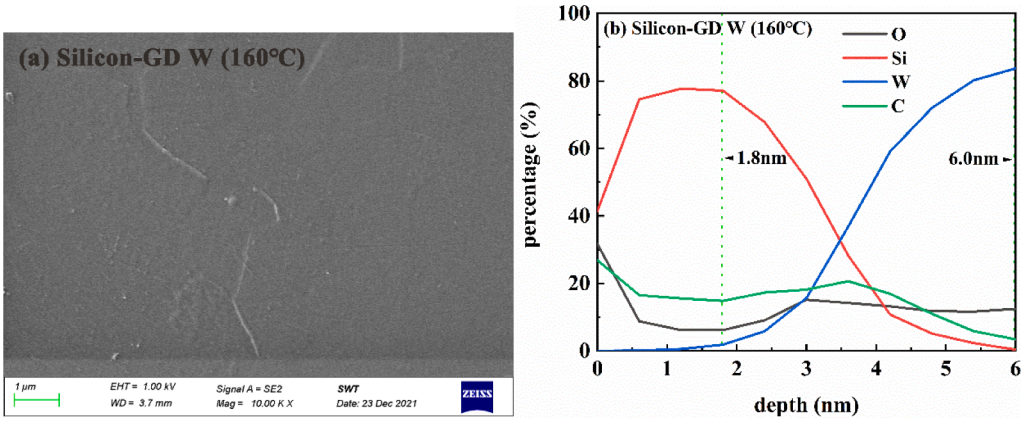

Fig. 6. The SEM images and the results of the XPS analysis after siliconization of the surface of the W samples, assisted by GD at 160 °C baking temperature: (a) the microstructure of the film; (b) distribution of the elements with film thickness.

The chemical properties of Si-coated samples assisted by GD are shown in Fig. 7(a-c). As described in the previous analysis, we selected six points at different depths beneath the sample surface. The Si 2P spectra of the film surface showed two peaks located at 99.72 eV and 102.60 eV, corresponding to Si (7(a)). From 1.2 nm to 4.8 nm, a Si peak was found at 99.72 eV. After 4.8 nm, other curves of Si 2P spectra became flat. In Fig. 7(c), from 2.4 nm to the surface of the W sample, the W 4f spectra showed two peaks located at 31.47 eV and 33.60 eV, corresponding to W and WO_2, which were similar to the results of the Si film formed by ICRF at 40 kW power. These findings showed that the W sample was cleaner when glow discharge was performed before siliconization.

4. Discussion

As described in Section 3.1, the Si film on the W surface formed at 160 °C baking temperature and the ICRF working power of 20 kW was smoother and more compact compared to the Si film formed at 60 °C. Impurities were removed from the surface before coating (See 2c and 2d) for increasing adhesion. As shown in Fig. 2(c and d), although, the thickness of the Si film at different baking temperatures were identical, the content of other species was lower in the normalized plot. The baking temperature of the W substrate influenced the adhesion and purity of the Si film. This was probably because the surface of the W substrate was cleaner at the higher baking temperature. The impurities with water were effectively desorbed from the surface when the W sample was baked at a high temperature. As shown in Fig. 8, the gaseous impurities released from the original W sample at 200 °C were analyzed by TDS. The results showed that the partial pressure of the released impurities of H_2O, N_2, CO_2, and H_2 increased with the increase the baking temperature. The content of H_2O released was more than that of the other molecules when the baking temperature of the W sample was maintained at 200 °C for a prolonged period. This indicated that the initial W sample absorbed a large quantity of H_2O and a small quantity of CO_2.

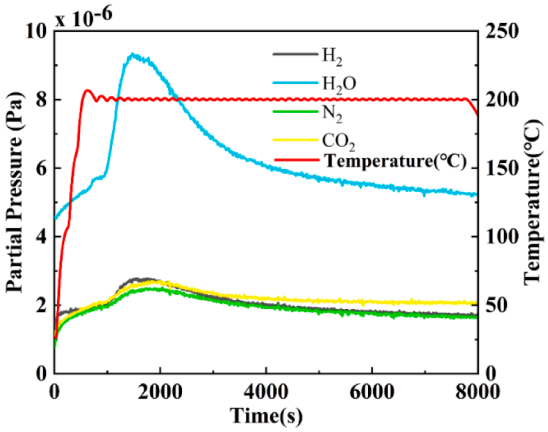

Fig. 8. The results of the TDS analysis of the initial W sample (baked at 200 °C).

The probable chemical reactions that occurred between Si and the gaseous impurities (H_2O and CO_2) during the Si-coating experiment are as follows:

$$Si(g) + 2H_2O(g) \xrightarrow{\Delta} SiO_2(s) + 2H_2(g)\ (350K, DG = -389.1\,kJ) \quad (1)$$

$$Si(g) + CO_2(g) \xrightarrow{\Delta} SiO_2(s) + C(s) \quad (350K, DG = -452.3\,kJ) \quad (2)$$

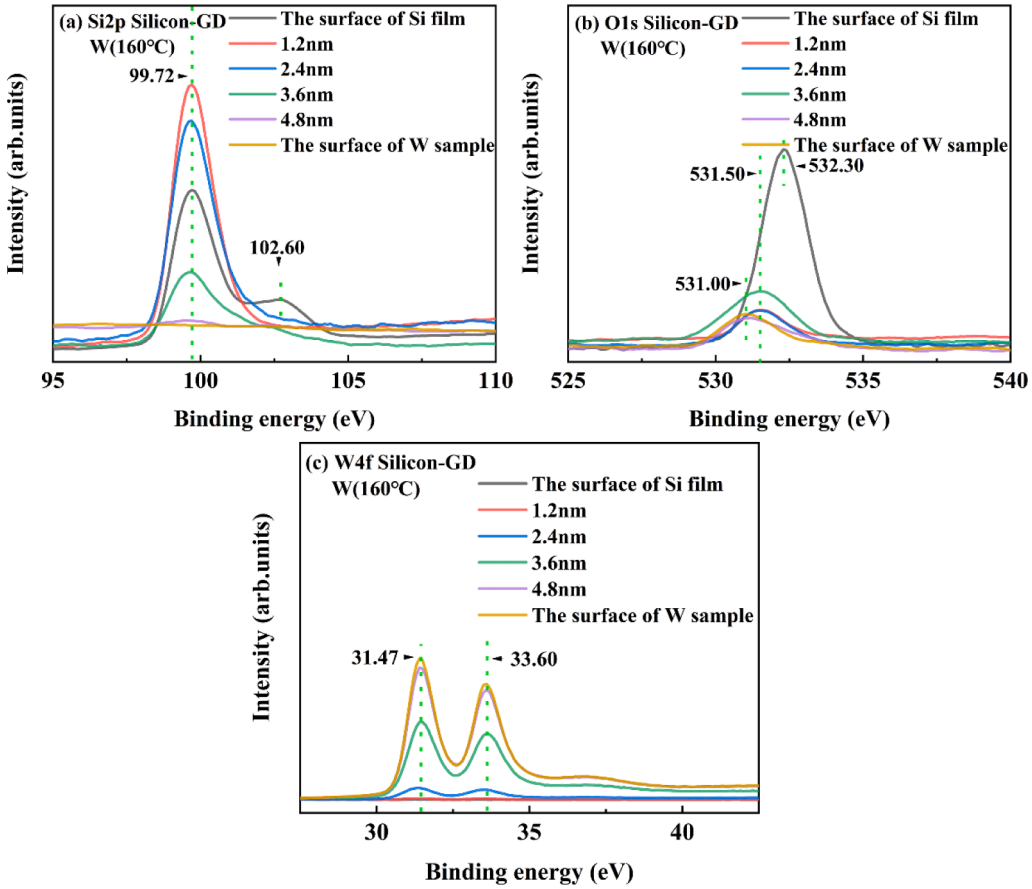

Fig. 7. The XPS spectra of siliconization of W samples assisted by GD at 160 °C baking temperature: (a) Si 2p spectra; (b) O 1 s spectra; (c) W 4f spectra.

The Gibbs free energy (ΔG) of Eqs. (1) and (2) was negative at 60 °C, which indicated that SiO_2 was formed when Si was exposed to H_2O and CO_2. Additionally, the results of the XPS analysis showed that the oxides of W were also distributed on the surface of the W substrate, as shown in Fig. 3(c). This was mainly because W reacted with oxygen. The possible reactions are as follows:

$$W(s) + 2H_2O(g) \xrightarrow{\Delta} WO_2(s) + 2H_2(s) \quad (350K, DG = -66.5\,kJ) \tag{3}$$

$$2W(s) + 2O_2(g) \xrightarrow{\Delta} 2WO_2(s) \quad (350K, DG = -1048.4\,kJ) \tag{4}$$

$$2W(s) + 3O_2(g) \xrightarrow{\Delta} 2WO_3(s) \quad (350\,K, DG = -1500.9\,kJ). \tag{5}$$

The ΔG of Eqs. (3), (4) and (5) was negative, which indicated that the W surface could be oxidized while baking the W substrate. These equations matched the results of XPS analysis, which showed that W oxides were present on the surface of the substrate in Figs. 3, 5, and 7. Thus, the oxides of SiO_2, WO_2, and WO_3 were formed when the W substrate was baked at 60 °C, which led to poor adhesion between the Si film and the W substrate, as shown in Fig. 3. Bubbles and folds were formed due to the dampening of the Si film, as shown in Fig. 2(a). The content of Si was lower than that of O due to the presence of several types of oxides, including SiO_2, WO_2, and WO_3, as shown in Fig. 2(c). The surface of the W substrate was cleaner when it was baked at 160 °C, which occurred because H_2O and CO_2 were partially released (Fig. 8). At this temperature, a smaller amount of WO_2 and WO_3 was formed on the surface of the W sample, and a smaller amount of SiO_2 was generated during the Si coating experiment, which resulted in a higher content of Si in the film and better adhesion between the Si film and the W substrate. Hence, no bubbles and folds appeared on the film and the content of Si on the film surface was higher than that of O and W, as shown in Fig. 2(b) and 2(d).

For ICRF discharge, the light brightness measured by camera from horizontal port was stronger with 40 kW ICRF discharge than that with 20 kW ICRF discharge, as shown in Fig. 9. The possible reason is that plasma density is proportional to the coupled RF power. When the plasma density becomes high enough with higher coupled RF power, the plasma waves can start propagating causing further ionization and plasma build-up along the torus. Due to the increase of both the electron and the He densities, it can increase particle removal rate when ICRF discharge cleaning is performed with the higher RF power. Similar results was also observed in the W7-AS, it was found higher working power was helpful to improve cleaning efficiency [27].

For Si coating assisted by 20 kW and 40 kW RF power, the thickness and characteristics of Si coated films were different. For the W sample baked at 60 °C, we compared the Si-coated films formed via ICRF at 20 kW and 40 kW. As shown in Fig. 4, the surface of the Si film was uniform and the thickness of the film increased to 4.5 nm from 20 kW to 40 kW. Additionally, the content of Si at 40 kW was higher than that at 20 kW. This was mainly due to two reasons. The first reason was that the cleaning capability of ICRF before Si coating was significantly higher when the working power was high. The adsorbed low-energy gaseous impurities, such as H_2O and CO_2, were released, and the W oxides on the surface of the W sample were decomposed and removed. This produced a cleaner surface at 40 kW than at 20 kW. These results strongly indicated that W was detected in the XPS analysis (Fig. 5(c)). Therefore, while performing Si coating with ICRF, the adhesion of the Si film at 40 kW working power was better than that at 20 kW when the baking temperature was 60 °C (Fig. 4(a) and 2(a)). A small amount of SiO_2 was detected on the surface of the W substrate, and the main component of the coating from 1.2 to 2.4 nm was Si. The content of Si was higher than that of O and W in the film, as shown in Fig. 4(b) and 5(a). In the W7-AS stellarator, higher working power was found to increase cleaning efficiency [27]. The Si and SiO_2 peaks were found in the Si 2p spectra (Fig. 5 (a)) because the Si film became slightly oxidized while being transferred to the XPS system in the air. The second reason was that the energy of Si^{4+} and $SiD_x^{(4-x)+}$ and flux increased significantly when the working power of the ICRF was increased. During siliconization via ICRF, SiD_4 was initially ionized to Si^{4+} and $SiD_x^{(4-x)+}$, and then, the ions moved to and were deposited on the first wall. As shown in Fig. 10(a), at 20 kW, the contents of the gases with a mass number of 28 (Si, N_2, and CO), 30 (SiD^{3+}), 32 (SiD_2^{2+} and O_2), and 34 (SiD_3^{1+}) were approximately 24 %, 9.3 %, 39.7 %, and 27 %, while the content of SiD_4 (mass number 36) was only 1 %. As shown in Fig. 10(b), SiD_4 was not detected. The contents of the gases with a mass number of 28, 30, 32, and 34 were 33 %, 6.5 %, 38.5 %, and 23 % at 20 kW. These results showed that higher working power increased the siliconization rate.

The evolution of working gases during siliconization via ICRF at 20 kW and 40 kW working power and 60 °C baking temperature is shown in Fig. 10. RGA was measured during the discharge. As the ICRF working power increased, the ion flux and energy also increased; thus, the number of ions that reached the sample surface was higher, and the time required for the ions to reach the sample surface was shorter, and the ions avoided being pumped away by the pumping system. This process led to the formation of a Si film that was thicker than that formed under the lower working power of ICRF, as shown in Fig. 2(c) and 4(b).

The Si particle influx per unit area onto the surface of the W sample can be described as:

$$\Gamma_i = n_e C_s \sin\theta \tag{6}$$

Here, n_e represents the edge plasma density, C_s represents the ion sound speed, and θ represents the angle of the magnetic field line with respect to the sample surface [28]. During the sample surface cleaning and siliconization, the magnetic field is only toroidal magnetic field. The angle of the magnetic field direction relative to the sample surface was fixed at

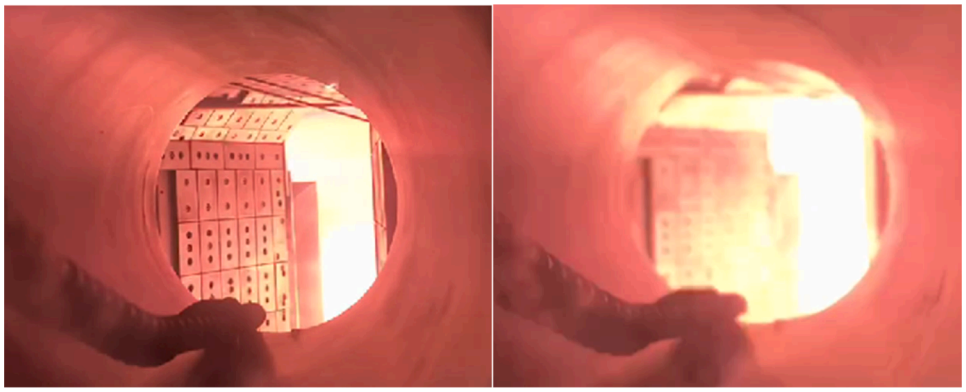

(a) (b)

Fig. 9. Comparison of light brightness with different RF power (a) 20 kW and (b) 40 kW.

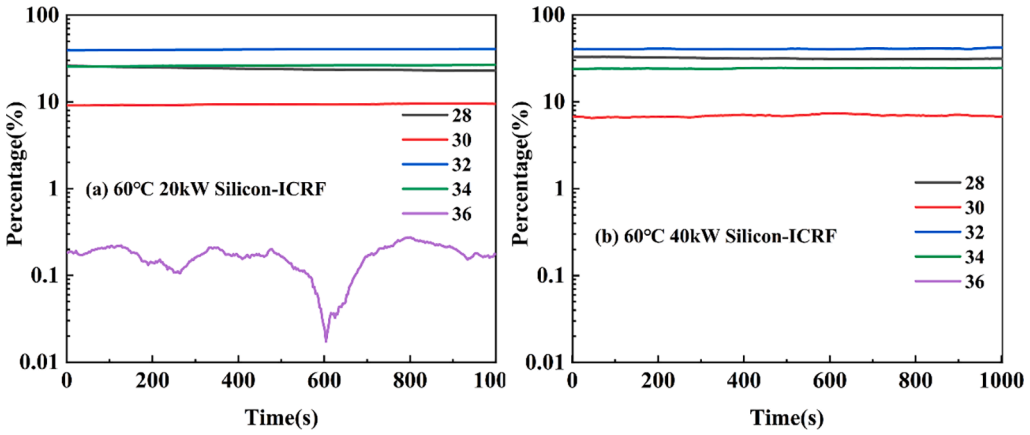

Fig. 10. The evolution of working gases during siliconization via ICRF at 60 °C and working power of (a) 20 kW and (b) 40 kW.

$\theta \sim 1.5°$. In Eq. (6), the ICRF under higher working power corresponded to higher gas ionization, which increased the ion density and temperature, thus increasing ion flux and the thickness of the coated film. In addition to the magnetic field angle, the influence of the magnetic field strength on cleaning and coating homogeneity is discussed here. The evolution of partial pressure of various gases during ICRF cleaning with different toroidal magnetic field (B_T = 0.5 T, 1.0 T, 2.0 T) is shown in Fig. 11. The partial pressure of various gases was almost kept constant under different toroidal magnetic field. The real-time photographs monitored by high-speed camera during ICRF cleaning discharge with different toroidal magnetic field, confirms that the ICRF plasma homogeneity is similar, except for the two slight toroidal bright belt located at the same major radial position with the ICRF cleaning antenna (R = 2.5 m) as shown in Fig. 12. Therefore, the homogeneity of wall cleaning has no obvious difference with different toroidal magnetic field strength.

During the Si film with ICRF discharge, it was proved that the film thickness was very uniform along the toroidal direction. The real time thickness of Si coated film analyzed by film thickness meter QMB (quartz crystal microbalance systems) during Si coating assisted by ICRF discharge, as shown in Fig. 13.Three QMBs located at C and J ports were used to evaluate the uniformity and coating rate. The major radius of QMB, QMB2 and QMB3 was 2.65 m, 2.73 m and 2.73 m respectively. It was confirmed that the growth of Si film was stable and the homogeneity of the coating was well by comparing the film thickness of the C and J ports.

Compared with ICRF discharge, the structure of the glow discharge system is relatively simple. Therefore, the glow discharge has become the routine discharge cleaning method in many tokamaks [18,29,30].

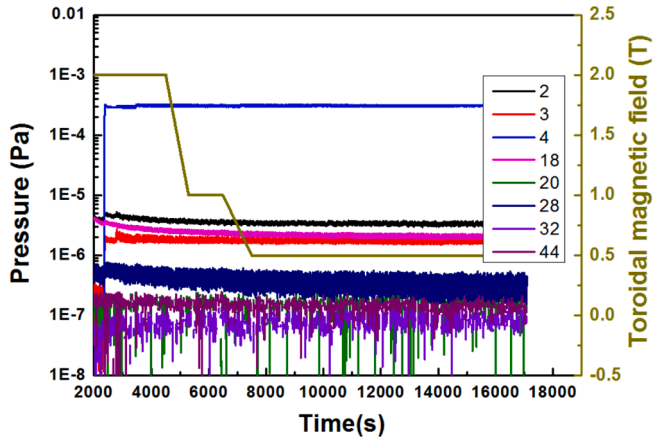

Fig. 11. The evolution of partial pressure of various gases during ICRF discharge with different toroidal magnetic field strength.

GDC discharge is more uniform for wall cleaning and coating in the vacuum vessel, as shown in Fig. 14. In EAST, four stainless steel anodes are fixed at the vessel wall of plasma vacuum vessel and the first wall of the whole device is a cathode [31]. The voltage between the anode and cathode is 1000 V when the plasma is breakdown and then it keeps at the 200 V during regular GDC discharge. DC glow discharge only relies on limited electric field and sheath potential to accelerate ions, the energy obtained by ions is limited to <10 eV. Meanwhile, the permanent presence of toroidal field between plasma discharges in fusion devices limits GDC cleaning application. For ITER device, GDC wall conditioning is still designed and applied when vent to air or during machine non-operation maintenance without magnetic field. The primary advantage of ICRF discharge is that it could be applied with the existing of the toroidal magnetic field. Compared with DC glow discharge, RF discharge has higher heating power (20–40 kW), and the electron and ion can obtain higher energy. It is reported that the electron temperature for helium RF plasmas is in the range 3–50 eV in the reference [32], which is helpful to remove high-energy impurities from the first wall surface.

Siliconization performed via GD at 160 °C produced a smoother and thicker coating than that obtained by performing ICRF at 20 kW and 160 °C. The content of Si was also higher, as shown in Fig. 2(b, c) and 4 (a, b). As described in Section 2, the glow discharge was normally set to run continuously, and it was performed using four fixed anodes (400 W for each anode) at 10^{-1} Pa. The ICRF discharge was performed using a set of antennas, 2 sets of 50 kW RF transmitters. Overall, it was more uniform than ICRF. During siliconization performed by ICRF discharge, the duty time and the working pressure were normally set at 0.5 s on/5 s off and 10^{-2} Pa, respectively. Although the working power of ICRF was higher than that of GD, the actual working duration of ICRF was about 10 min, which was considerably shorter than the working duration of GD (110 min). Thus, the efficiency of GD was higher than that of ICRF, which was confirmed in EAST. As shown in Fig. 7(c), the W peaks were detected in the W 4f spectra. The pattern was similar to that observed for siliconization via ICRF, which indicated strong adhesion of the Si film with the W substrate and a high content of Si in the film.

The working gas pressure of GD was about 0.1 Pa, which was 10 times greater than that of ICRF. The evolution of the working gas during siliconization of the W sample via ICRF and GD at 20 kW and 1.6 kW working power and 160 °C baking temperature is shown in Fig. 15. The partial pressure of various gases during ICRF and GD was monitored by residual gas analyzers (RGA). Because the coating duration of siliconization assisted by He-ICRF and He-GD was about only 110 mins, and it would produce little influence on sensitivity of RGA. As shown in Fig. 15 (a), the gas pressure of gases with a mass number of 28 (Si, N_2, and CO), 30 (SiD^{3+}), 32 (SiD_2^{2+} and O_2), and 34 (SiD_3^{1+}) was approximately 1.33 $\times 10^{-6}$ Pa, 5.52 $\times 10^{-7}$ Pa, 2.34 $\times 10^{-6}$ Pa, and 1.59 $\times 10^{-6}$ Pa, while the

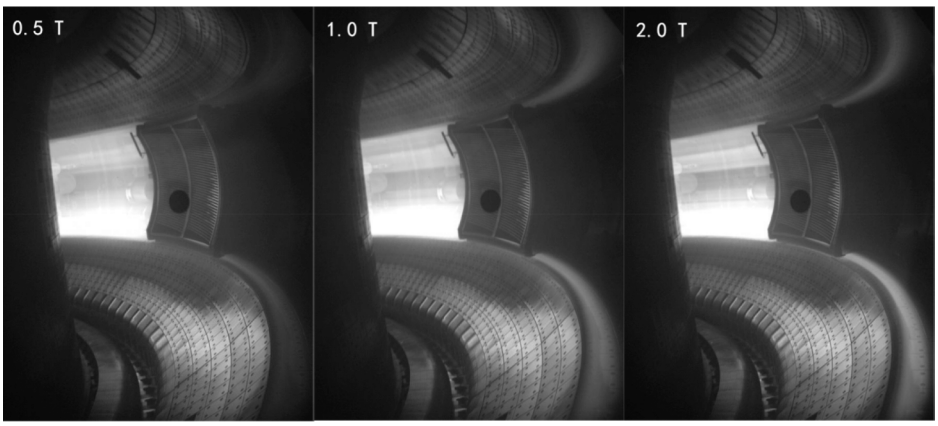

Fig. 12. Real-time photographs monitored by the high-speed camera during ICRF discharge with different toroidal magnetic field: (a) BT = 0.5 T; (b) BT = 1.0 T; (c) BT = 2.0 T.

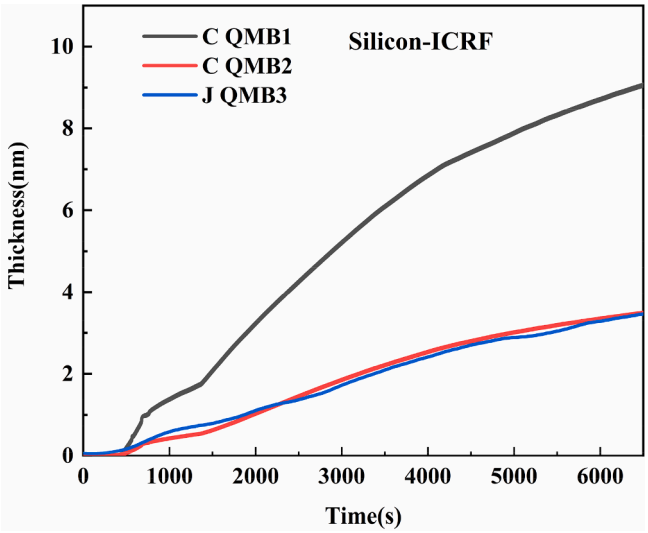

Fig. 13. Real-time thickness analyzed by film thickness meter.

Fig. 14. Picture of glow discharge cleaning took by the visible camera.

gas pressure of SiD_4 was around 1.00×10^{-8} Pa. As shown in Fig. 15(b), the gas pressure of the gases with a mass number of 28, 30, 32, and 34 was 5.67×10^{-6} Pa, 4.28×10^{-6} Pa, 1.75×10^{-5} Pa, and 1.08×10^{-5} Pa, while the gas pressure of SiD_4 was 3.55×10^{-7} Pa. During siliconization via GD, the content of ionized Si increased significantly, which indicated that GD enhanced the ionization process. Additionally, SiD_4 could be further ionized, and the ionized particles were easily deposited on the first wall due to the long operation time of GD. This indicated that more particles were ionized during siliconization via GD than that during siliconization via ICRF coating. The main component of the film was Si. These reasons favor the formation of Si films via GD, as shown in Fig. 2 (c, d) and 6(b).

In addition, we have made an estimation on the Si sputtering by He during the ICRF Si coating using the ERO code [33]. According to the local plasma conditions, the ne is lower than 1×10^{17} m^{-3} and Te is about 5 eV. The erosion rate of Si by He sputtering is around 0.005 nm/s, which can't be neglected compared to the coating rate. It provides a reasonable explanation why the thickness of Si coated film is only few nanometers via 110 min coating. Next step, if possible, we will try to reduce He ratio to < 80 %, and further investigate the Si film characteristics.

5. Conclusion

To reduce the strong plasma-tungsten wall interaction and promote plasma steady-state operation, siliconization using 10 % SiD_4 + 90 % He via ICRF or GD was performed in EAST. The characteristics of the film with various Si coating conditions, including baking temperature, ICRF power, and discharge types, were investigated and compared. The conclusions might be summarized as follows:

(1) A higher baking temperature of the W sample released more physically absorbed gaseous impurities, especially water. More compact and smoother Si films were obtained at a higher temperature.
(2) Increasing the ICRF working power from 20 kW to 40 kW further increased the ratio of Si/O in the Si film. Thus, higher working power helped to remove surface oxides and other compounds. It also increased the silane ionization rate, and more $SiD_x^{(4-x)+}$ ions were coated on the surface of the W sample. This, in turn, increased the thickness of the Si film.
(3) Siliconization via GD was more uniform and thicker, and the ratio of silicon/oxygen (Si/O) was considerably higher than that obtained by siliconization via ICRF. These changes were due to a

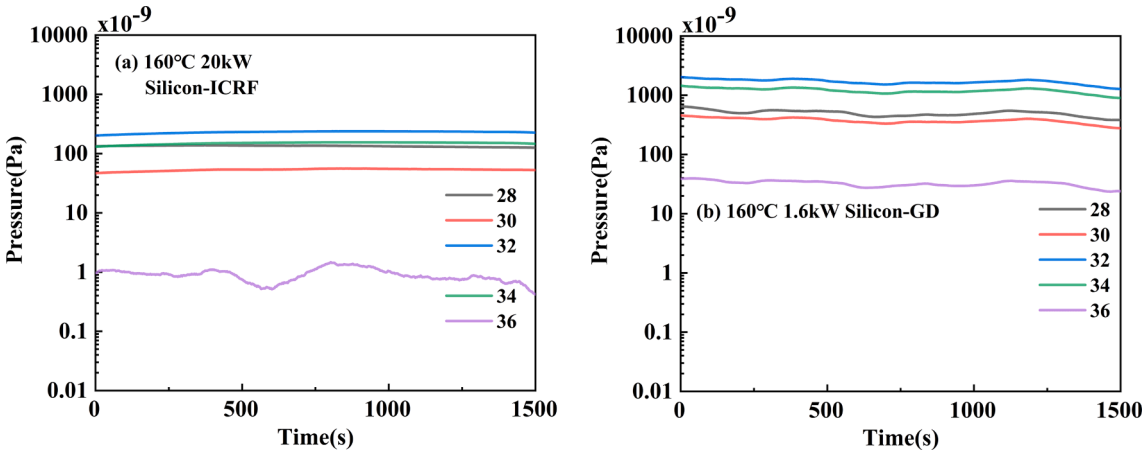

Fig. 15. The evolution of the working gas during siliconization via ICRF and GD at 160 °C: (a) ICRF coating at 20 kW, (b) GD coating at 1.6 kW.

higher working gas pressure, longer coating duration, and more homogeneous discharge under GD.

CRediT authorship contribution statement

Yanhong Guan: Conceptualization, Investigation, Methodology, Writing – original draft, Data curation. **Guizhong Zuo:** Investigation, Methodology, Project administration, Writing – review & editing, Supervision. **Xiancai Meng:** Investigation, Visualization, Software, Data curation. **Wei Xu:** Software, Investigation. **Yaowei Yu:** Data curation, Formal analysis. **Ming Huang:** Investigation, Methodology. **Lin Li:** Data curation, Investigation, Methodology. **Jiansheng Hu:** Project administration, Validation, Supervision.

Declaration of Competing Interest

The authors declare that they have no known competing financial interests or personal relationships that could have appeared to influence the work reported in this paper.

Data availability

Data will be made available on request.

Acknowledgements

This research is funded by the National Key Research and Development Program of China (2017YFE0301100, 2022YFE03130000), National Nature Science Foundation of China (11905138, 11905148, 11905254), and the U.S. Dept. of Energy contract DE-AC02–09CH11466 and grant DE-SC0016553. Users with Excellence Program of Hefei Science Center CAS (2020HSC-UE010). The Institute of Energy, Hefei Comprehensive National Science Center under Grant Nos. 21KZS202 and 21KZS208 and Interdisciplinary and Collaborative Teams of CAS.

References

[1] S. Banacloche, et al., Socioeconomic and environmental impacts of bringing the sun to earth: A sustainability analysis of a fusion power plant deployment, Energy 209 (2020) 118460, https://doi.org/10.1016/j.energy.2020.118460.
[2] H. Han, et al., A sustained high-temperature fusion plasma regime facilitated by fast ions, Nature 609 (7926) (2022) 269–275, https://doi.org/10.1038/s41586-022-05008-1.
[3] G. Federici, et al., Plasma-material interactions in current tokamaks and their implications for next step fusion reactors, Nucl. Fusion 41 (12) (2001) 1967, https://doi.org/10.1088/0029-5515/41/12/218.
[4] A. Kallenbach, E.M.T.J.N. Fusion, Overview of ASDEX Upgrade results, Nucl. Fusion 57 (10) (2017) 102015, https://doi.org/10.1088/1741-4326/aa64f6.
[5] X. Litaudon, et al., Overview of the JET results in support to ITER, Nucl. Fusion 57 (10) (2017) 102001, https://doi.org/10.1088/1741-4326/aa5e28.
[6] H. Zohm, et al., Overview of ASDEX Upgrade results, Nucl. Fusion 43 (12) (2003) 1570, https://doi.org/10.1088/0029-5515/43/12/004.
[7] D.M. Yao, et al., Design, R&D and commissioning of EAST tungsten divertor, Physica Scripta T167 (2016), https://doi.org/10.1088/0031-8949/2015/t167/014003.
[8] R. Pitts, et al., A full tungsten divertor for ITER: Physics issues and design status, J. Nucl. Mater. 438 (2013) S48–S56, https://doi.org/10.1016/j.jnucmat.2013.01.008.
[9] G. Zuo, et al., Comparison of various wall conditionings on the reduction of H content and particle recycling in EAST, Plasma Phys. Controlled Fusion 54 (1) (2011) 015014, https://doi.org/10.1088/0741-3335/54/1/015014.
[10] H. Jiansheng, et al., Brief review to the interactions into plasma and walls in magnetic controlled fusion devices, J. Univ. Sci. Technol. China 50 (9) (2020) 1193, https://doi.org/10.3969/j.issn.0253-2778.2020.09.001.
[11] G. Jackson, et al., Boronization in Diii-D, J. Nucl. Mater. 196 (1992) 236–240, https://doi.org/10.1016/S0022-3115(06)80038-3.
[12] R. Majeski, et al., Enhanced energy confinement and performance in a low-recycling tokamak, Phys. Rev. Lett. 97 (7) (2006), 075002, https://doi.org/10.1103/PhysRevLett.97.075002.
[13] H. Esser, et al., Plasma discharge fuelling by trimethylboron-a new wall conditioning technique, Nucl. Fusion 32 (2) (1992) 278, https://doi.org/10.1088/0029-5515/32/2/i08.
[14] M. Saidoh, et al., Initial boronization of JT-60U tokamak using decaborane, Jpn. J. Appl. Phys. 32 (7R) (1993) 3276, https://doi.org/10.1143/jjap.32.3276.
[15] V.K. Alimov, et al., Characterization of aB/C: H films deposited from different boron containing precursors, J. Nucl. Mater. 196 (1992) 670–675, https://doi.org/10.1016/S0022-3115(06)80120-0.
[16] K. Nishimura, et al., Effects of Boronization in LHD, J. Plasma Fusion Res. 79 (12) (2003) 1216–1217, https://doi.org/10.1585/jspf.79.1216.
[17] U. Schneider, et al., Boronization of ASDEX, J. Nucl. Mater. 176 (1990) 350–356, https://doi.org/10.1016/0022-3115(90)90071-t.
[18] V. Rohde, et al., Wall conditioning in ASDEX Upgrade, J. Nucl. Mater. 363 (2007) 1369–1374, https://doi.org/10.1016/j.jnucmat.2007.01.200.
[19] G.Z. Zuo, et al., Comparison of various wall conditionings on the reduction of H content and particle recycling in EAST, Plasma Phys. Control. Fusion 54 (1) (2012) 015014, https://doi.org/10.1088/0741-3335/54/1/015014.
[20] D. Mansfield, et al., Enhancement of Tokamak Fusion Test Reactor performance by lithium conditioning, Phys. Plasmas 3 (5) (1996) 1892–1897, https://doi.org/10.1063/1.871984.
[21] G. Zuo, et al., Lithium coating for H-mode and high performance plasmas on EAST in ASIPP, J. Nucl. Mater. 438 (2013) S90–S95, https://doi.org/10.1016/j.jnucmat.2013.01.014.
[22] R. Maingi, et al., Overview of L-H power threshold studies in NSTX, Nucl. Fusion 50 (6) (2010) 064010, https://doi.org/10.1088/0029-5515/50/6/064010.
[23] C. Li, et al., Deuterium retention characteristics in Li film by coating and during flowing liquid Li limiter operation in experimental advanced superconducting tokamak, Plasma Phys. Controlled Fusion 63 (1) (2020) 015001, https://doi.org/10.1088/1361-6587/abc396.
[24] L. Peng, et al., Improvement of plasma performance with wall conditioning in the HL-1M tokamak, Nucl. Fusion 38 (8) (1998) 1137, https://doi.org/10.1088/0029-5515/38/8/302.
[25] U. Samm, et al., Plasma edge physics with siliconization in TEXTOR, J. Nucl. Mater. 220 (1995) 25–35, https://doi.org/10.1016/0022-3115(94)00444-7.
[26] F. Ding, et al., Overview of plasma–material interaction experiments on EAST employing MAPES, J. Nucl. Mater. 455 (1–3) (2014) 710–716, https://doi.org/10.1016/j.jnucmat.2014.09.017.
[27] R. Brakel, et al., ICRF wall conditioning experiments in the W7-AS stellarator, J. Nucl. Mater. 290 (2001) 1160–1164, https://doi.org/10.1016/s0022-3115(00)00554-7.

[28] G. Zuo, et al., Mitigation of plasma–material interactions via passive Li efflux from the surface of a flowing liquid lithium limiter in EAST, Nucl. Fusion 57 (4) (2017) 046017, https://doi.org/10.1088/1741-4326/aa5ea0.
[29] T. Härtl, et al., Optimization of the ASDEX Upgrade glow discharge, Fusion Eng. Des. 124 (2017) 283–286, https://doi.org/10.1016/j.fusengdes.2017.04.029.
[30] Z. Zhou, et al., Design and application of GDC on EAST Tokamak, Fusion Eng. Des. 86 (9–11) (2011) 1599–1602, https://doi.org/10.1016/j.fusengdes.2011.03.052.
[31] J. Hu, et al., Vacuum and wall conditioning system on EAST, Fusion Eng. Des. 84 (12) (2009) 2167–2173, https://doi.org/10.1016/j.fusengdes.2009.03.016.
[32] J. Li, et al., Wall conditioning towards the utilization in ITER, J. Nucl. Mater. 415 (1) (2011) S35–S41, https://doi.org/10.1016/j.jnucmat.2010.10.048.
[33] R. Ding, et al., Material migration studies with an ITER first wall panel proxy on EAST, Nucl. Fusion 55 (2) (2015) 023013, https://doi.org/10.1088/0029-5515/55/2/023013.